



# Recovery of Valuable Metals from Spent $\text{Al}_2\text{O}_3$ -Based Catalysts by Sodium Carbonate Roasting and Water Leaching

XIN LIANG,<sup>1</sup> JUNJIE TANG,<sup>2,3</sup> LAISHI LI,<sup>1,4</sup> and YUSHENG WU<sup>1</sup>

1.—School of Materials Science and Engineering, Shenyang University of Technology, Shenyang 110870, China. 2.—School of Environmental and Chemical Engineering, Shenyang University of Technology, Shenyang 110870, China. 3.—e-mail: tangjunjie1987@sut.edu.cn. 4.—e-mail: lilaishi@sut.edu.cn

This paper reports a comprehensive recovery of valuable metals from spent  $\text{Al}_2\text{O}_3$ -based catalysts using sodium carbonate roasting and water leaching. In all experimental parameters, roasting is one of the most critical influences on the leaching effect. During the roasting of sodium carbonate, insoluble  $\text{NiAl}_2\text{O}_4$  and  $\alpha\text{-Al}_2\text{O}_3$  are converted to soluble  $\text{NaAlO}_2$ , which can be leached by water. Then, Al, Ni, and V were recovered by leaching solution and residue, respectively. The experimental results showed that Al and V leaching rates were 99.64% and 99.24%, respectively, under the optimal leaching conditions. Moreover, the simple metal composition in the leachate and residue is more favorable for metal recovery than the direct recovery of Al and Ni from the spent  $\text{Al}_2\text{O}_3$ -based catalyst. Adding  $\text{Ba}(\text{OH})_2$ , which is stoichiometric with V, to the leachate allows the recovery of V first. Subsequently,  $\text{Al}(\text{OH})_3$  precipitation was obtained by adding the appropriate amount of hydrochloric acid dropwise, and  $\gamma\text{-Al}_2\text{O}_3$  was obtained by calcination. The residue was acid-leached using sulfuric acid again, and after the reaction,  $\text{Ni}(\text{OH})_2$  was recovered by adding excess NaOH.  $\text{Ni}(\text{OH})_2$  was heated to a certain temperature to obtain NiO. The recoveries of Al and Ni were 98.68% and 96.31%, respectively, during the whole experiment.

## INTRODUCTION

Catalysts are critical in the petrochemical industry since they are responsible for many reactions. The share of refining catalysts in the world's industrial catalysts is growing yearly.<sup>1</sup> The structure and active components of the catalyst are irreversibly affected as the operation period, and the number of uses rise, resulting in the deactivation of the catalyst, which is eventually disposed of as solid waste.<sup>2</sup> Because of the enormous number of heavy metals included in the consumed catalysts, random disposal of spent catalysts harms the environment and humans and wastes resources for the metals in the consumed catalysts. Spent catalysts have a high metal content, making them a valuable secondary resource.<sup>3</sup> To meet the development needs of

industrialized countries, the mining of primary metal ores has also intensified. Therefore, to reduce ore mining and environmental pollution, it is crucial to extract metals from spent catalysts and carry out harmless treatment.<sup>4,5</sup>

Currently, there are two main methods for recovering metals from spent catalysts: hydrometallurgy and pyrometallurgy.<sup>6,7</sup> Due to reduced energy consumption, fewer hazardous gas emissions, and less waste formation, hydrometallurgical procedures are preferable to pyrometallurgical techniques in recovering valuable metals from spent catalysts, according to most of these assessments.<sup>8,9</sup> Hydrometallurgy mainly includes acid leaching,<sup>10,11</sup> alkali leaching,<sup>12,13</sup> oxidation leaching,<sup>14,15</sup> bioleaching,<sup>16,17</sup> oxide roasting leaching,<sup>18,19</sup> and so on. Acid leaching is one of the most common leaching methods. Most metals or metal oxides can be dissolved in the leaching solution.<sup>20</sup> The leaching behavior of Mo, Co, and Al following the addition of oxidants to sulfuric acid to overcome the

(Received February 15, 2023; accepted May 15, 2023; published online June 12, 2023)

hydrophobicity of sulfides and sulfur elements in the catalyst matrix was researched by Barik et al. Under ideal leaching circumstances, Al extraction rates were 99.87%, 96.25%, and 11.03%, respectively.<sup>21</sup> Nguyen et al. used HCl to recover Mo and Co from spent desulfurization catalysts, and the total recoveries of Mo and Co reached 96% and 93%, respectively, under optimal conditions.<sup>22</sup> Moreover, Lai et al. combined mixed acid leaching with a fluidized bed point solution process.<sup>23</sup> It was found that the highest leaching rates of the target metals were achieved when concentrated HNO<sub>3</sub>: H<sub>2</sub>SO<sub>4</sub>: HCl was mixed in a 2:1:1 ratio by volume, with 99%, 99%, and 90% for V, Ni, and Mo, respectively. However, most metals or metal oxides are soluble in acid, making subsequent separation more complex and the quality of the recovered metal low, limiting the use of acid leaching.

Using pyrometallurgical roasting processes may be more effective in recovering valuable metals, especially for catalysts that use Al<sub>2</sub>O<sub>3</sub> as a carrier. Wang et al.<sup>24</sup> reported a process for recovering valuable metals from spent catalysts by blank roasting and NaOH leaching. To convert  $\gamma$ -Al<sub>2</sub>O<sub>3</sub> to  $\alpha$ -Al<sub>2</sub>O<sub>3</sub> by roasting, the thermodynamics of the roasting process was systematically analyzed. The  $\alpha$ -Al<sub>2</sub>O<sub>3</sub> was made to be retained in the solid phase during the alkaline leaching process, thus allowing the separation of valuable metals for leaching. Kim et al. used sodium carbonate roasting and boiling water immersion to recover V and W from spent selective catalytic reduction catalysts. The ultimate leaching rates of V and W were 46% and 92%, respectively.<sup>25</sup> Ye et al. used microwave sodium salt roasting method to recover Mo from spent desulfurization and hydrogenation catalysts to achieve in situ sulfur fixation. While achieving the maximum harmless treatment of the spent catalyst, the Mo leaching rate was as high as 99%.<sup>26</sup> Li et al. studied the leaching of Mo and V under the condition that 10% NaCl was added to the spent desulfurization and hydrogenation catalyst for auxiliary roasting. The leaching rates of Mo and V under the optimal conditions were 93.5% and 87.5%, respectively.<sup>27</sup> Therefore, roasting leaching plays a positive role in the selective recovery of metals and has the characteristics of a high metal recovery rate and purity.

As the literature mentioned above shows, developing an efficient method for recovering spent catalysts is crucial. Most of the valuable metals have been recovered in some studies, but the carrier Al<sub>2</sub>O<sub>3</sub> has not been recovered, which also causes environmental pollution and resource waste. Therefore, this study uses sodium carbonate roasting to selectively leach and recover Al, Ni, and V with stable phase compositions. The process parameters affecting the recovery rate were studied in detail, and the optimum process conditions were established for Al, Ni, and V recovery. The process is characterized by changing the phase transformation

mechanism of spent catalyst ore, revealing the reaction mechanism of sodium carbonate with  $\alpha$ -Al<sub>2</sub>O<sub>3</sub> and NiAl<sub>2</sub>O<sub>4</sub> during the roasting process and promoting the practical application of pyro-combined hydrometallurgical technology in the field of solid waste resource recovery.

## EXPERIMENTAL

### Materials and Pretreatment

Spent Al<sub>2</sub>O<sub>3</sub>-based catalyst was provided by Huludao Oil Refining Chemical Plant in China. It should be mentioned here that the spent catalysts used in this study did not contain Mo. The spent catalysts were crushed, ground, and sieved (< 100 mesh after grinding) before the experiments and then dried in a desiccator at 105°C for 24 h for the experiments. Chemical reagents were of analytical grade, including Na<sub>2</sub>CO<sub>3</sub>, NaOH, Ba(OH)<sub>2</sub>, HCl, H<sub>2</sub>SO<sub>4</sub>, and H<sub>2</sub>O<sub>2</sub>. They were used as received from Sinopharm Chemical Reagent Co., Ltd. All of the chemicals used in the experiment were not purified before use. The pH meter used for pH adjustment is from the Shanghai Leici PHS-3E model. The high-speed centrifuge used in the liquid–solid separation stage was from Xiang Yi TG16-WS. Deionized water from the GWB-2 ultrapure water device of Beijing Puyan General Instrument Co., Ltd., was used in all experiments.

### Experimental Method

The roasted spent catalyst is mixed and crushed in a ball mill with sodium carbonate in a specific ratio. The mixed spent catalyst powder was roasted in a muffle furnace. After roasting, transfer the sample to a three-necked flask, add a certain amount of distilled water, and put the three-necked flask into it after the constant magnetic stirrer has been heated to the required temperature. The residue after the reaction was separated from the filtrate, and the pulp density used was 10% unless otherwise specified. The leaching residue was then repeatedly washed with distilled water, dried at 105°C for 24 h, and characterized for its chemical composition and content. The chemical composition and content of the spent catalyst and each leaching residue were analyzed by ICP-OES. The formula for calculating the target metal leaching efficiency is as follows:

$$\% \text{Leaching} = 1 - \frac{W_1 M_1}{W_s M_s} \quad (1)$$

where  $W_s$  is the percentage of metal in the original spent catalyst and  $M_s$  is the mass of the original spent catalyst;  $W_1$  is the percentage of metal in the leach residue and  $M_1$  is the mass of the leach residue.

The filtrate is first separated from the filter residue in the comprehensive recovery of metals. The filtered residue was added to the H<sub>2</sub>SO<sub>4</sub>

solution, and after the reaction, the reddish brown Fe(OH)<sub>3</sub> and Ni(OH)<sub>2</sub> could be obtained by adding NaOH to adjust the pH, respectively. Ba(OH)<sub>2</sub> was added to the separated filtrate to obtain Ba<sub>3</sub>(VO<sub>4</sub>)<sub>2</sub>. Filter again and add NaOH to adjust the pH to get the precipitate. The precipitate was roasted to 700°C to obtain the γ-Al<sub>2</sub>O<sub>3</sub> carrier for the catalyst again.

### Characterization and Analysis

The distribution and content of metals in the spent Al<sub>2</sub>O<sub>3</sub>-based catalyst and the spent catalyst after roasting were determined by X-ray fluorescence spectrometer (XRF, ARL PERFORM'X USA). Chemical analysis was carried out by EDTA complexation titration.<sup>28</sup> Sulfate was estimated by the gravimetric method with 5% BaCl<sub>2</sub> solution.<sup>29</sup> The spent catalyst mineral phase is analyzed by X-ray diffraction (XRD, XRD-7000X, Japan). TG-DTA curve ( $T = 30\text{--}1000^\circ\text{C}$ , heating rate 10°C/min, a nitrogen atmosphere) was obtained by vacuum-sealed synchronous TG-DTA thermal analyzer (STA 449 F5 Jupiter, Germany). Surface morphology and composition of spent catalysts, leaching residues, and obtained products were obtained using a scanning electron microscope (SEM, Gemini SEM 300, Japan) equipped with an energy-dispersive X-ray spectrometer (EDS, Oxford Instruments). The concentration of metal ions in the leachate was detected using ICP-AES (Prodigy Plus, Leeman, USA).

## RESULTS AND DISCUSSION

### Spent Al<sub>2</sub>O<sub>3</sub>-Based Catalyst Roasting

#### Characterization of the Spent Al<sub>2</sub>O<sub>3</sub>-Based Catalyst

According to the SEM and EDS results in Fig. 1a, the surface roughness of the spent Al<sub>2</sub>O<sub>3</sub>-based catalyst is mainly composed of large mass particles, and the main elements present on the surface are Al, Ni, V, and Fe. The XRF results show that the spent catalyst has a complex composition with many heavy metals such as Al, Ni, and V, as shown in Table I. Small amounts of metals such as Na, Si, and Ca are also present in the spent catalyst, which may be due to the trace metals left by the oil attached to the spent catalyst. Moreover, XRD patterns show that the main phases of the spent catalyst are α-Al<sub>2</sub>O<sub>3</sub> (PDF card no. 71-1683), NiAl<sub>2</sub>O<sub>4</sub> (PDF card no. 10-0339), and Fe<sub>2</sub>O<sub>3</sub> (PDF card no. 33-0664) as presented in Fig. 1b. Phases for other metals were not detected, probably because of the lower metal content. The formation of NiAl<sub>2</sub>O<sub>4</sub> may be due to the formation of many insoluble by-products during the air oxidation roasting of the spent catalyst in the refinery, which increases the difficulty of subsequent recovery.<sup>30,31</sup>

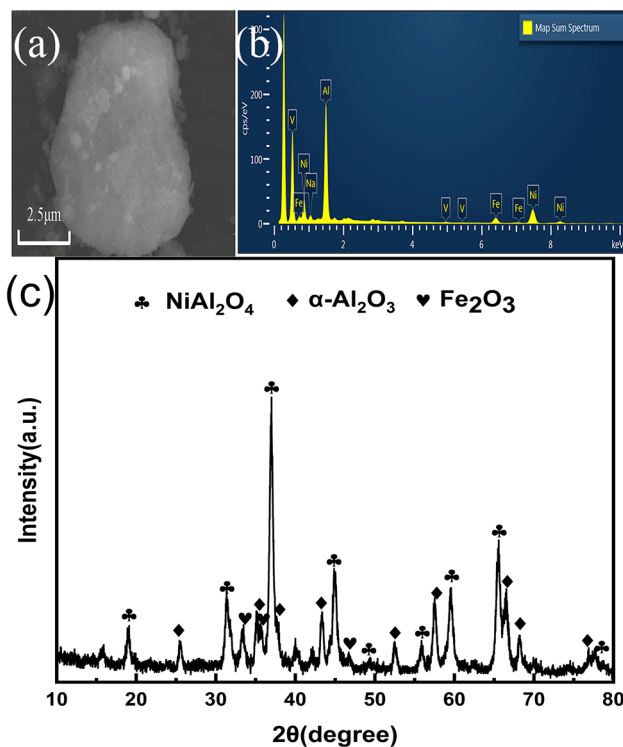


Fig. 1. (a) SEM, (b) EDS and (c) XRD patterns of original spent Al<sub>2</sub>O<sub>3</sub>-based catalysts.

#### Thermodynamic Analysis of the Roasting Process

A certain amount of sodium carbonate is added to the spent catalyst for roasting, and the occurrence of metal and sodium carbonate in the roasting process is as follows:

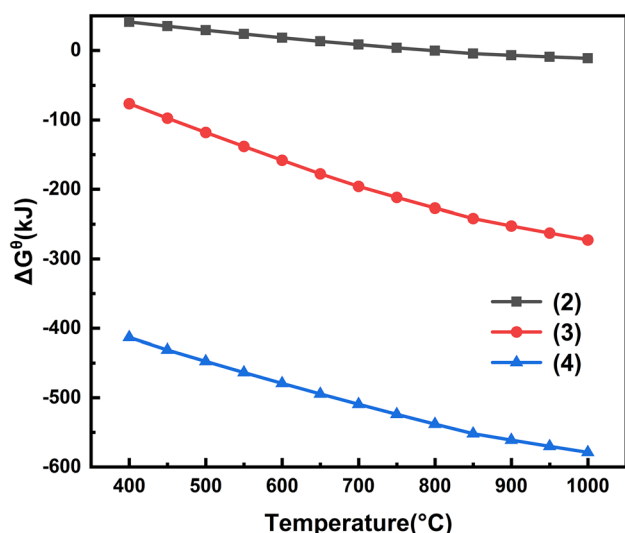


Generally, sodium carbonate reaches a molten state at 854°C and starts to react with metals (Al, V, and so on) in the spent catalyst. Sodium carbonate will decompose into sodium oxide and CO<sub>2</sub>, and the decomposition rate is slow.<sup>32,33</sup> Figure 2 shows the Gibbs free energy calculated based on the above reaction as a function of temperature (this data was calculated by HSC software). The Gibbs free energy of reaction (2) is negative when the temperature is > 800°C, so to ensure that reaction (2) can be carried out, the reaction temperature should be > 800°C. The Gibbs free energy of reactions (3) and (4) is always < 0 at 400–1000°C. It shows that when the temperature is > 800°C, Al<sub>2</sub>O<sub>3</sub> is converted to the corresponding product by reaction with Na<sub>2</sub>CO<sub>3</sub>. The results of the TG-DTA tests and thermodynamic calculations provide the theoretical basis and data support for the determination of the subsequent reaction temperature.

**Table I. XRF analysis of the original spent  $\text{Al}_2\text{O}_3$ -based catalyst**

Compound	$\text{Al}_2\text{O}_3$	NiO	$\text{Na}_2\text{O}$	$\text{Fe}_2\text{O}_3$	$\text{V}_2\text{O}_5$	$\text{SiO}_2$	CaO	$\text{P}_2\text{O}_5$	LOI
Wt.%	74.92	11.49	2.67	2.36	0.99	1.64	0.74	0.86	1.97

LOI Loss on ignition at 1323 K.

Fig. 2. The relationship between temperature and  $\Delta G^\theta$ .

### Roasting Mechanisms

Samples of the spent  $\text{Al}_2\text{O}_3$ -based catalyst mixed with sodium carbonate were subjected to TG–DTA testing to verify the accuracy of the baking temperature. The test was performed in a nitrogen atmosphere at a heating rate of  $10^\circ\text{C}/\text{min}$ . Figure S1 (see supplementary material) shows the TG–DTA curve of the original spent catalyst, where the mass of the spent catalyst decreases with increasing temperature in the range of  $100\text{--}200^\circ\text{C}$ . Continue to increase the temperature and quality without significant change. No exothermic peaks exist in the DTA curve. The TG–DTA curve is shown in Fig. 3, where the mass decreases to about 86.25 wt.% during the roasting process. From 100 to  $200^\circ\text{C}$ , the quality of the raw material decreases slightly, which is caused by the evaporation of water in the raw material. There is an apparent endothermic peak at  $861.2^\circ\text{C}$  compared with the thermodynamic results of the HSC Chemistry 6.0 software and the melting point of sodium carbonate, indicating that  $\text{Al}_2\text{O}_3$  begins to react with sodium carbonate. However, heat is released during the reaction of  $\text{Al}_2\text{O}_3$  with  $\text{Na}_2\text{CO}_3$ . Sodium carbonate melts and absorbs a large amount of heat at  $851^\circ\text{C}$ . Therefore, a heat absorption peak rather than an exothermic peak is generated at  $861.2^\circ\text{C}$ . The mass of the feedstock decreases rapidly because of the production of  $\text{CO}_2$ .

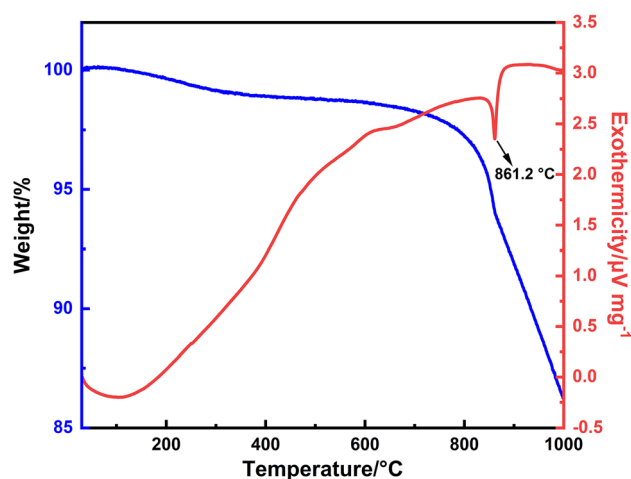


Fig. 3. TG–DTA curve of spent catalyst mixed with sodium carbonate (Sodium carbonate addition: 1.5).

The curve stabilizes when  $900^\circ\text{C}$  is reached, indicating the end of the reaction. Therefore, the reaction temperature was determined to be  $900^\circ\text{C}$  by TG–DTA and thermodynamic calculation results.

During the roasting of sodium carbonate, the change of phase in the spent  $\text{Al}_2\text{O}_3$ -based catalyst determines the extent to which the reaction proceeds.<sup>34</sup> According to the thermodynamic theoretical calculations and TG–DTA test results, the phase transformation process of the sample at  $800\text{--}1000^\circ\text{C}$  was characterized. As shown in Fig. 4, the peak  $\alpha\text{-Al}_2\text{O}_3$  was 19.06, 31.24, 37.04, 45.04, 49.26, 55.84, 59.52, and  $65.48$  degrees, respectively, and there was no  $\gamma\text{-Al}_2\text{O}_3$ . In addition, Ni exists in the form of  $\text{NiAl}_2\text{O}_4$ , and the content of V in the spent catalyst is low and cannot be found in the XRD analysis. When the spent catalyst is calcined with sodium carbonate at  $800^\circ\text{C}$ , there is no significant change in other phases except the characteristic diffraction peak of sodium carbonate. It is because the reaction kinetics between  $\text{Al}_2\text{O}_3$  and sodium carbonate cannot be satisfied at this temperature. When the calcination temperature was increased to  $900^\circ\text{C}$ ,  $\text{NiAl}_2\text{O}_4$  and  $\alpha\text{-Al}_2\text{O}_3$  reacted with sodium carbonate. The corresponding characteristic diffraction peaks completely disappeared and were transformed into NiO and  $\text{NaAlO}_2$  phases, indicating sufficient reaction. When the temperature was further raised to  $1000^\circ\text{C}$ , there was no significant change in the test results. The phase transition



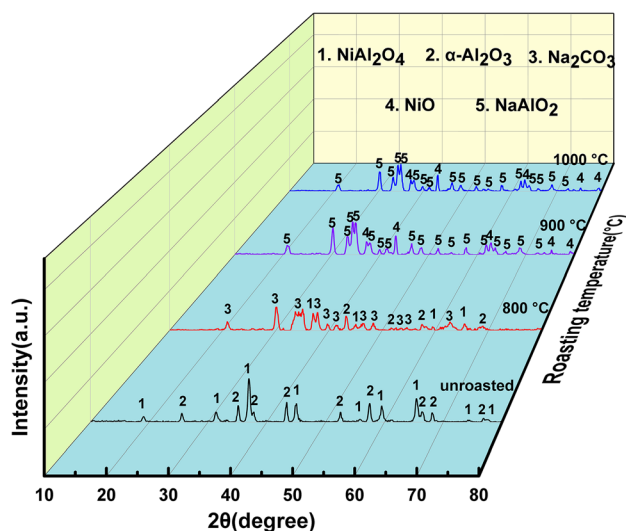


Fig. 4. XRD patterns of spent catalysts at different roasting temperatures. (Roasting time: 4 h, Sodium carbonate addition: 1.5, Heating rate: 10°C/min).

seemed to have been completed, and NaAlO<sub>2</sub> and NiO became stable phases.

We also characterized the microscopic morphology of the mixed roasting of sodium carbonate and spent catalyst at different roasting temperatures by SEM, as shown in Fig. 5. At 600°C, the surface of large-size particles of the spent catalyst produces small bulk sintered matter, which may be due to the reaction of V, Si, P, and other substances in the spent catalyst with sodium carbonate at this temperature. When the calcination temperature increased from 600°C to 700°C, the surface did not change significantly, indicating that no reaction occurred at the calcination temperature of 800°C, and more sintering products accumulated on the surface of the spent catalyst, indicating that sodium carbonate began to participate in the reaction. However, many large particles are still on the surface, indicating that the reaction is incomplete and the calcination temperature needs to be increased. As the roasting temperature increased to 900°C, many tiny holes appeared on the surface. There was no significant difference in roasting at 1000°C compared to 900°C, proving that the reaction had proceeded completely. At this time, Al in the spent catalyst has been transformed into NaAlO<sub>2</sub>.

#### Effect of Roasting Temperature

Figure 6a shows the effect of roasting time on the leaching efficiency. Since the selective Ni of sodium carbonate roasting does not react with it, only the effects on Al and V leaching efficiency are studied. The conditions of water leaching are leaching temperature: 95°C, leaching time: 2 h, L/S: 10 mL/g, and stirring speed: 300 rpm. In the range of 600–1000°C, the leaching efficiency of Al and V is higher with the increase in temperature. The actual

roasting temperature is higher than the theoretical roasting temperature, which may be because the reaction is about to complete when the roasting temperature is higher. At 1000°C, Al and V leaching rates were 99.46% and 98.98%, respectively. Compared with the direct sulfuric acid in and out, the method of roasting and leaching using Na<sub>2</sub>CO<sub>3</sub> can effectively leach aluminum because, at 1000°C, the alumina has wholly reacted with sodium carbonate and is converted into NaAlO<sub>2</sub> with high solubility. The results show that the addition of Na<sub>2</sub>CO<sub>3</sub> is practical for the separation of Al and Ni. To ensure the complete reaction, the optimal roasting temperature is determined to be 1000°C.

#### Effect of Roasting Time

To study the effect of roasting temperature on the leaching of Al and V, the roasting temperature was fixed at 900°C, and the amount of sodium carbonate was 1.5. The conditions of water leaching are leaching temperature: 95°C, leaching time: 2 h, L/S: 10 mL/g, and stirring speed: 300 rpm. The roasting time has a significant effect on the leaching efficiency of Al and V. The experimental results are shown in Fig. 6b. The results showed that the leaching rates of Al and V increased significantly with the roasting time in the range of 1–4 h. The leaching rates were 98.86% and 98.4%, respectively, which proved the good roasting effect. Therefore, the roasting time was kept at 4 h in the subsequent experiments.

#### Effect of Sodium Carbonate Addition

To investigate the effect of sodium carbonate addition on the roasting effect, experiments were conducted at a roasting temperature of 900°C and a roasting time of 4 h, with sodium carbonate addition in the range of 1–2. The amount of sodium carbonate added is the ratio of the stoichiometric number of sodium carbonate to the aluminum in the spent catalyst. The conditions of water leaching are leaching temperature: 95°C, leaching time: 2 h, L/S: 10 mL/g, and stirring speed: 300 rpm. The leaching efficiency of Al affects the subsequent acid leaching to dissolve Ni and Fe and reduce the content of Al in the acid leach solution. Therefore, the content of sodium carbonate needs to be increased to leach out as much Al as possible. The experimental results are shown in Fig. 6c. When the addition of sodium carbonate reaches 1.5, the leaching rate of Al increases rapidly to 98.24%. The leaching rate of V increases insignificantly. Therefore, the addition amount of 1.5 was chosen as the best parameter.

### Spent Al<sub>2</sub>O<sub>3</sub>-Based Catalyst Water Leaching

#### Effect of Leaching Time on Leaching Efficiency

In addition, the effect of leaching time was investigated. Other process parameters were fixed:

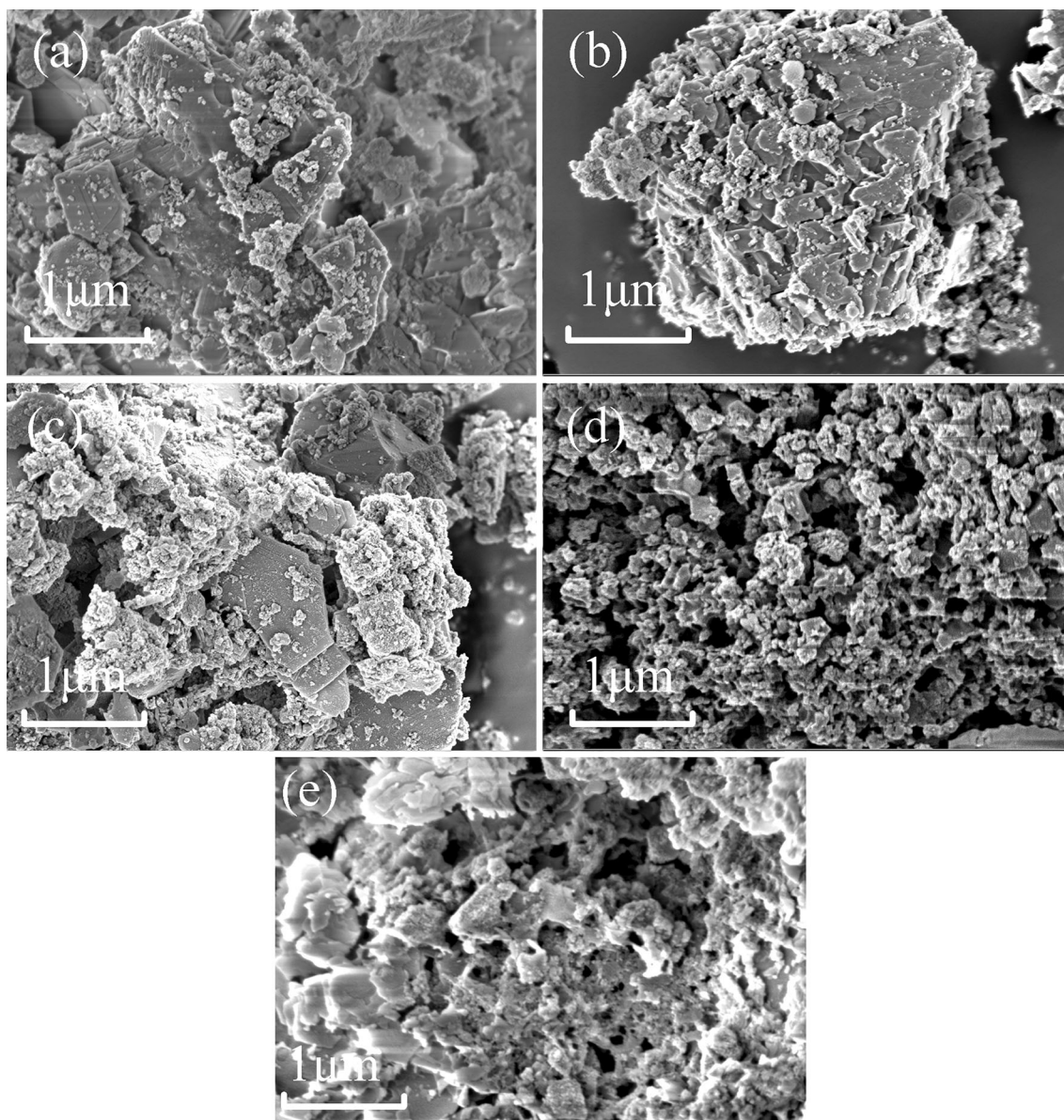


Fig. 5. SEM characterization at (a) 600°C, (b) 700°C, (c) 800°C, (d) 900°C and (e) 1000°C. (Roasting time: 4 h, Sodium carbonate addition: 1.5).

a leaching temperature of 75°C, L/S of 10 g/mL, and stirring speed of 300 rpm. The results are shown in Fig. 7a. This indicates that the leaching of Al and V was not significantly affected by the leaching time, and the leaching efficiencies were 96.72% and 97.4% for Al and V, respectively, when the leaching time was 2 h.

#### *Effect of L/S on Leaching Efficiency*

Subsequently, the effect of L/S on leaching was investigated, and the experimental results are shown in Fig. 7b. It is obvious that the leaching of Al and V is more influenced by L/S, which may be related to the fact that the samples are denser after roasting. Therefore, a larger L/S is more favorable

for better leaching of Al and V. An L/S of 7 mL/g is a good choice.

#### *Effect of Leaching Temperature on Leaching Efficiency*

Unlike other reported methods using acid–base leaching, this paper uses water as a leaching agent to leach the valuable metals from the roasted samples. The water solubility of  $\text{NaAlO}_2$  and  $\text{Na}_3\text{VO}_4$  is good, so they can be easily dissolved in the leaching solution. The effects on Al and V were investigated by varying the leaching temperature at 65–95°C, keeping other parameters at a leaching time of 2 h, a L/S of 10 g/mL, and a stirring speed of 300 rpm. The results are shown in Fig. 7c. When

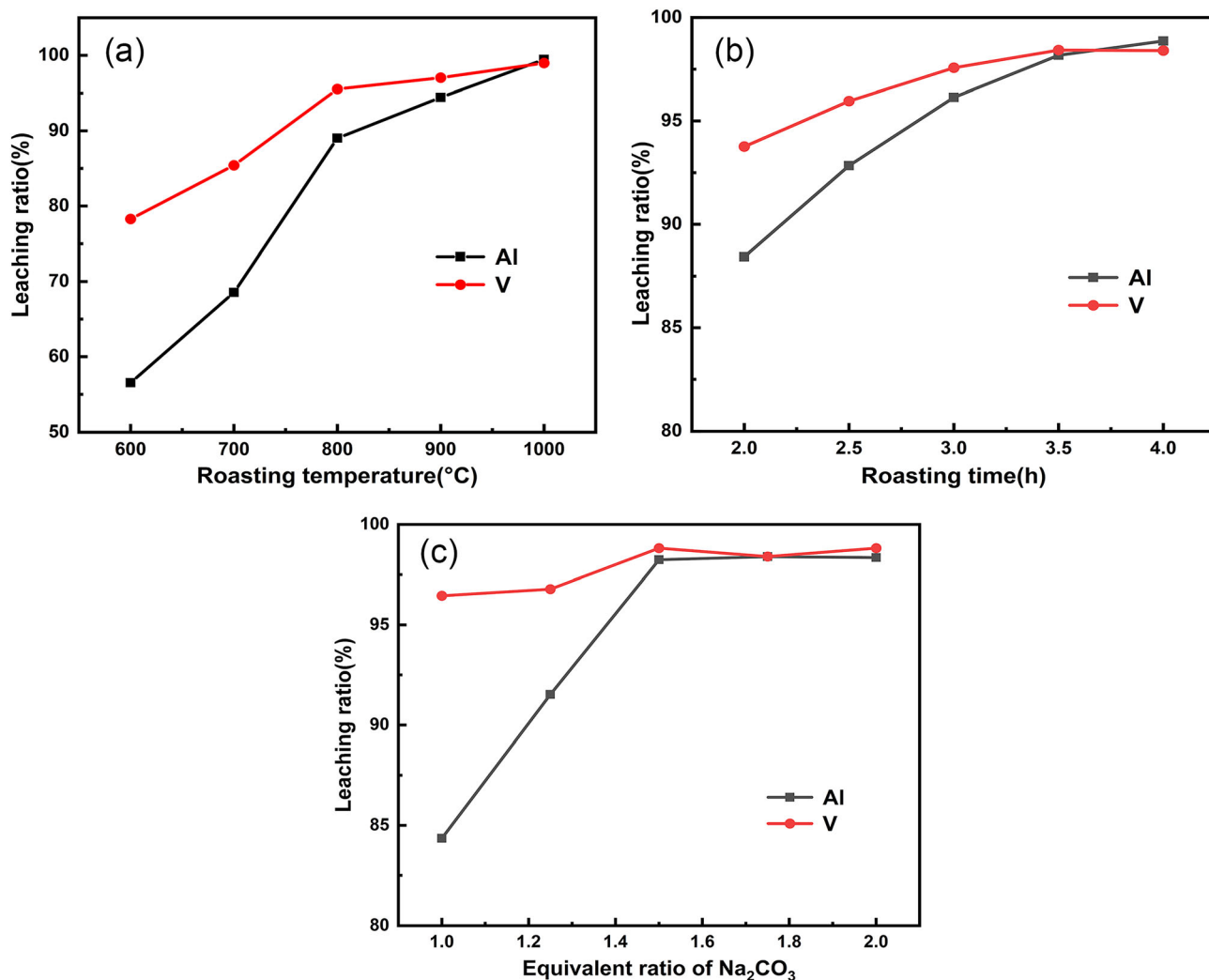


Fig. 6. Effect of (a) roasting temperature, (b) roasting time and (c) equivalent ratio of  $\text{Na}_2\text{CO}_3$  on the leaching effect of Al and V.

the leaching temperature reached  $75^\circ\text{C}$ , Al and V leaching rates were 97.6% and 97.6%, respectively. With the increased leaching temperature, the change in leaching efficiency was not noticeable, so  $75^\circ\text{C}$  was chosen as the best leaching temperature.

#### Effect of Stirring Speed on Leaching Efficiency

Finally, we carried out another experiment to check the leaching efficiency of Al and V under different stirring speed (200–400 rpm) conditions. As seen in Fig. 7d, the stirring speed has little effect on the leaching of both metals. When the stirring speed reached 200 rpm, Al and V leaching rates were  $> 94\%$ . The leaching efficiency of V did not change significantly throughout the process due to the low content of V, which was relatively easy in the leaching process. Contrarily, Al increased with the stirring speed, and the leaching efficiency of Al was 97.04% when it reached 350 rpm.

#### Characterization of leaching residue

To investigate the component changes of the roasting and leaching processes of the spent  $\text{Al}_2\text{O}_3$ -based catalysts, the analysis of roasting slag and leaching slag was analyzed. Figure S2 shows the XRD analysis under three different conditions. The XRD characterization results show that the residue phase is mainly NiO. Due to the low content of other elements, no other phases were found. Subsequently, SEM and EDS analyses were performed on the leach residue, as shown in Fig. S3. The analysis results show that the spent catalyst shows a fine granular spherical shape, and Al and V react well with sodium carbonate. The presence of V is no longer observed on the surface. Meanwhile, the content of Ni increases significantly, which also agrees with the XRD results. Subsequently, the residual phase was also characterized using XRF, and the results are shown in Table S1. Al and V were leached entirely out compared to the initially spent catalyst. The leachate and residue are recovered separately for further separation and recovery.



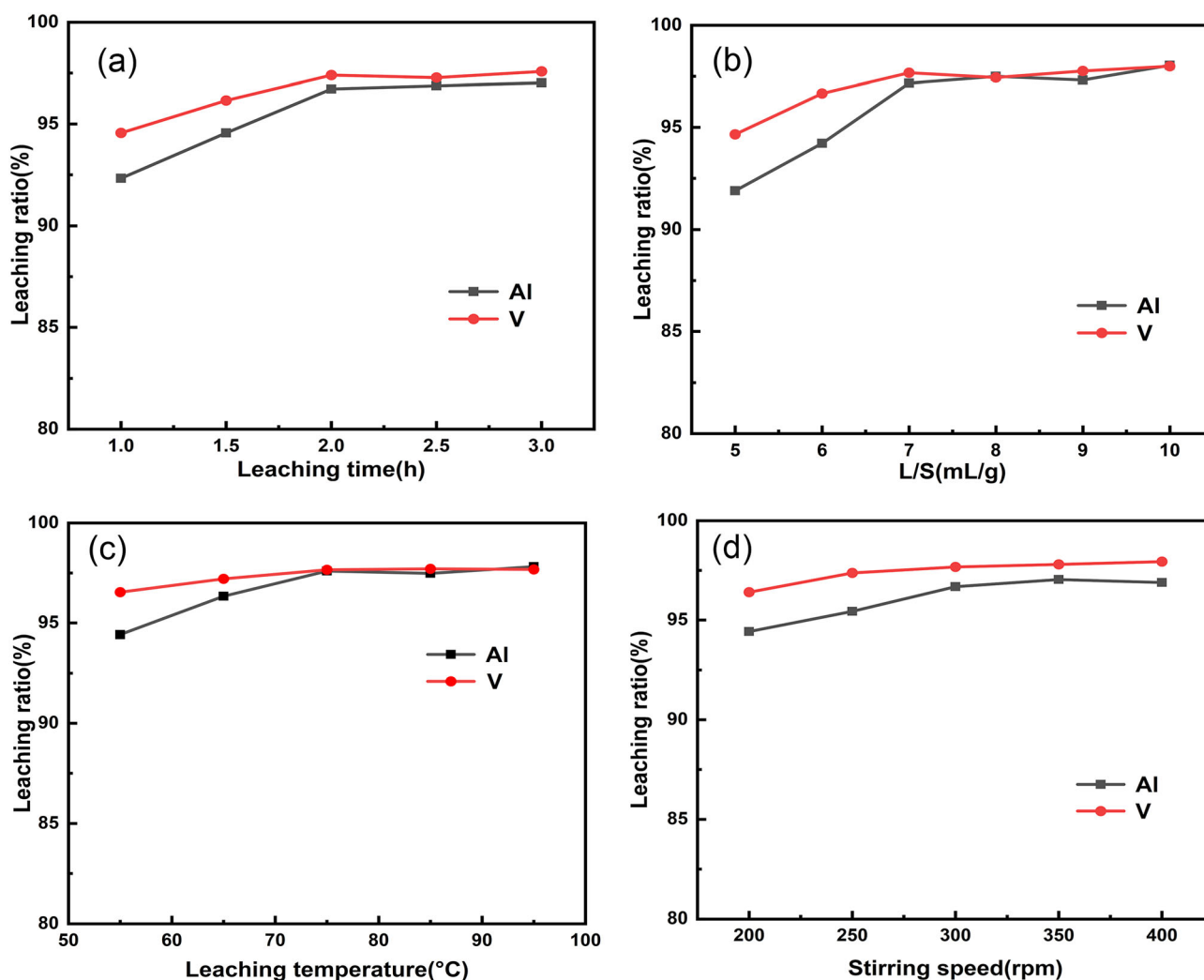


Fig. 7. Effect of (a) leaching time, (b) L/S, (c) leaching temperature, and (d) stirring speed on the leaching effect of Al and V.

### Recovery of Aluminum from Leaching Solution

To obtain high purity, Al one should first remove V from the leachate since  $\text{Ba}_3(\text{VO}_4)_2$  has very low solubility in water. In the recovery process, V was recovered by the dropwise addition of  $\text{Ba}(\text{OH})_2$ .<sup>35</sup> Under 40°C, reaction time of 30 min, and chemical reaction measurement of  $\text{Ba}(\text{OH})_2$ , the precipitation rate of V can be 95.84%.  $\text{Ba}(\text{OH})_2$  has no side effect on the decomposition of sodium aluminate solution.

The leachate after water leaching was collected using a beaker, and the acid method was used to obtain boehmite precipitation by adjusting the pH by adding hydrochloric acid dropwise. The accuracy of pH adjustment was achieved using a pH meter. The white precipitate was obtained by adjusting the pH to the pH range of the aluminum ion precipitate, and the white precipitate obtained was a milky white suspension colloid. The chemical reaction equation that occurred was as follows:



The precipitation was characterized by XRD and obtained as  $\text{AlOOH}$ . The results are shown in Fig. 8a.  $\text{AlOOH}$  is the precursor of  $\gamma\text{-Al}_2\text{O}_3$ , which can be roasted to obtain  $\gamma\text{-Al}_2\text{O}_3$  and re-prepare the carrier of the catalyst.<sup>36</sup> The  $\text{AlOOH}$  was calcined at 800°C to obtain  $\gamma\text{-Al}_2\text{O}_3$  with a purity of 97.42% (Supplementary Table. S2). The obtained  $\gamma\text{-Al}_2\text{O}_3$  was characterized by XRD as shown in Fig. 8b with PDF cards of 74-2206, and the experimental results were consistent with those of Zhang et al.<sup>37</sup> The obtained  $\gamma\text{-Al}_2\text{O}_3$  can be reused for the preparation of catalysts, achieving the recycling of carrier resources.<sup>38</sup>

### Recovery of Nickel from the Residue

Table S1 shows that the main components in the residue are Ni and Fe, which can be recovered by acid leaching and precipitation of Ni. Considering the strong oxidation of nitric acid, the leaching efficiency of Ni is lower than that of sulfuric acid. At the same time, the generated  $\text{Ni}(\text{NO}_3)_2 \cdot 6\text{H}_2\text{O}$  is a



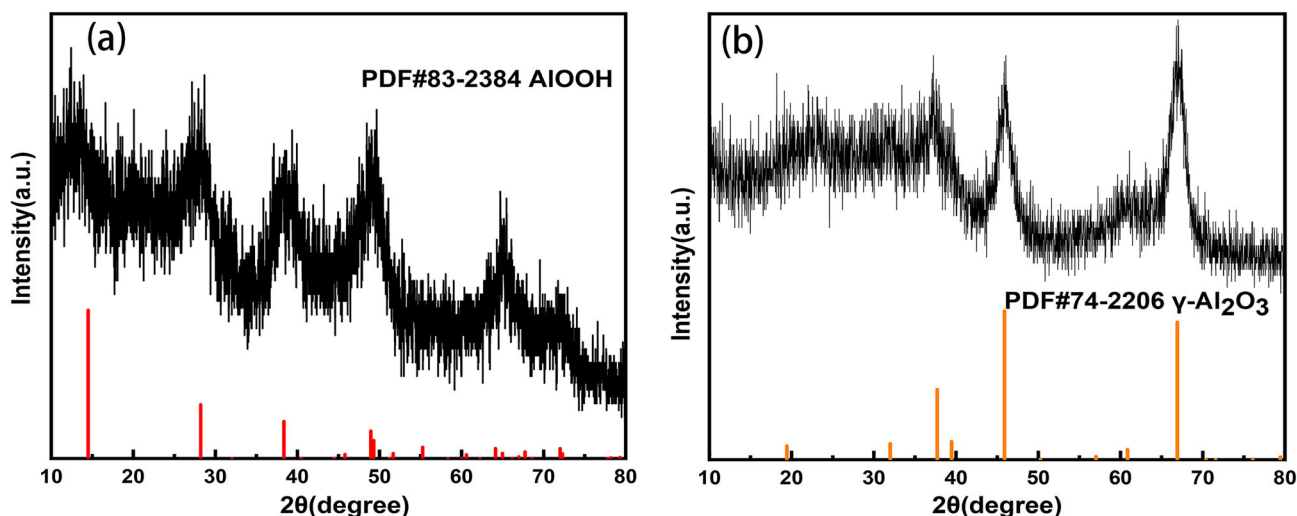


Fig. 8. XRD patterns of (a) recovered AlOOH and (b)  $\gamma$ -Al<sub>2</sub>O<sub>3</sub> obtained at 800°C.

toxic substance that is hazardous to human health. Therefore, sulfuric acid was chosen as the leaching agent. In addition, the leaching effect of hydrochloric acid on nickel was not significant.<sup>39</sup>

#### *Effect of leaching temperature on leaching efficiency*

Figure S4(a) shows the leaching efficiency of Ni in the residue at different leaching temperatures. The other parameters were fixed by varying the leaching temperature to 40–90°C. The leaching temperature strongly influences the leaching of metals, and leaching efficiency is low at leaching temperatures < 60°C, which provides inadequate reaction thermodynamics. When the temperature was increased to 60°C, Ni leaching rates increased to 98.22%. Continuing to increase the leaching temperature had little effect on the leaching efficiency of Ni. However, the reaction of NiO with sulfuric acid at 60°C is an exothermic reaction:  $\text{NiO} + \text{H}_2\text{SO}_4 = \text{NiSO}_4 + \text{H}_2\text{O}$ ,  $\Delta H = -105.325 \text{ kJ/mol}$ . Therefore, the leaching temperature of 60°C was used to leach Ni effectively.

#### *Effect of Leaching Time on Leaching Efficiency*

The leaching efficiency of nickel increased with the increase of leaching time, and the leaching efficiency of nickel could reach 92.83% after 3 h. Continuing to increase the concentration had no significant effect on the leaching of nickel (Supplementary Fig. S4(b)). Therefore, the leaching time was kept at 3 h during the subsequent experiments.

#### *Effect of Sulfuric Acid Concentration on Leaching Efficiency*

The sulfuric acid concentration is critical for Ni leaching, and the effect on Ni was tested in the range of 1–3 M. The results are shown in Fig. S4(c). When the sulfuric acid concentration was increased from 1 to 2 M, the leaching efficiency of Ni increased

from 72.46% to 97.26%. The sulfuric acid concentration influences Ni and Fe because of the simple metal composition in the residue and easy leaching. As the concentration of sulfuric acid increases, the dissolution efficiency of Fe increases with it, and the leaching of Fe should be controlled to reduce the difficulty of subsequent separation. Therefore, 2 M is the most suitable concentration.

#### *Effect of L/S on Leaching Efficiency*

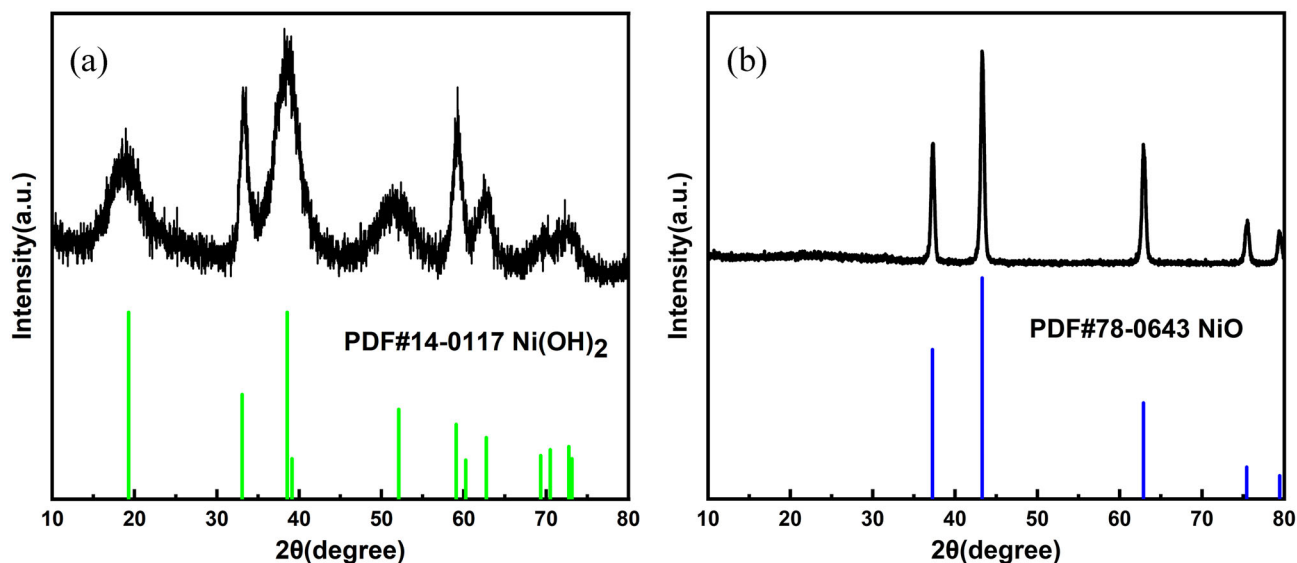
The leaching efficiency of nickel increased with the increase of L/S, and the resultant increase of surface L/S favored the leaching of nickel. When L/S was increased to 6 mL/g, the leaching efficiency of nickel could reach 98.68% (Supplementary Fig. S4(d)). Therefore, L/S was kept at 6 mL/g during the subsequent experiments.

### **Recovery and Characterization of Nickel**

H<sub>2</sub>O<sub>2</sub> is added to the leachate to ensure that all Fe<sup>2+</sup> is converted to Fe<sup>3+</sup>. The leaching solution after acid leaching was characterized by ICP-AES to detect the concentration of metal ions in the liquid phase, and the results are shown in Table II. The metal ions in the liquid phase were mainly Ni and Fe, with concentrations of 0.3642 mol/L and 0.0269 mol/L, respectively. Figure S5 shows the species distribution of Ni and Fe in the leachate at different pH conditions. The acid leaching solution obtained from the above optimal leaching process was recovered, and Ni and Fe were separated by dropwise addition of NaOH. A small amount of flocculent reddish-brown precipitate started to be produced when the pH reached about 2.9. The pH is kept at 5 to avoid the loss of Ni. Subsequently, the solution was recovered by separating Fe(OH)<sub>3</sub> through a centrifuge. The purity of nickel hydroxide was then characterized using XRF, as shown in Table S3. The characterization results show that

**Table II. The concentration of ions in the sulfuric acid leaching solution**

Element	Ni <sup>2+</sup>	Mg <sup>2+</sup>	Fe <sup>2+</sup>	Ca <sup>2+</sup>	Si <sup>2+</sup>
Concentration, mol/L	0.3642	0.0069	0.0269	0.0034	0.006

Fig. 9. XRD pattern of the recovered (a) Ni(OH)<sub>2</sub> and (b) NiO.

the main component of the recovered product is nickel oxide, and its purity can reach 98.177% (Supplementary Fig. S3). The obtained PDF cards of Ni(OH)<sub>2</sub> (PDF card no. 14-0117) are in agreement with the literature results, as shown in Fig. 9a.<sup>40</sup> Then, Ni(OH)<sub>2</sub> was roasted at 400°C to obtain NiO. The NiO was characterized by XRD, as shown in Fig. 9b. The obtained product is consistent with the position of the diffraction peak of NiO (PDF card no. 78-0643).<sup>41</sup>

The results of the study also confirm that the high efficiency and purity of aluminum and nickel recovery make it an efficient closed-loop integrated recovery process route. The recovery efficiencies of aluminum and nickel were 98.68% and 96.31%, indicating that almost all aluminum and nickel were recovered. Therefore, aluminum and nickel can be separated effectively by the proposed sodium carbonate roasting and water leaching. A process flow diagram for the leaching and recovery of valuable metals from spent Al<sub>2</sub>O<sub>3</sub>-based catalysts was obtained through a series of experimental studies, as shown in Fig. 10.

## CONCLUSION

This paper presents a comprehensive and efficient integrated recovery process for the closed-loop recovery of Al, Ni, and V from spent Al<sub>2</sub>O<sub>3</sub>-based catalysts. A process for separating and recovering Al, Ni, and V

from spent Al<sub>2</sub>O<sub>3</sub>-based catalysts is reported based on the characterization of phase transitions and compositions at different temperatures. Valuable metals are effectively separated by sodium carbonate roasting and water leaching, and the elemental composition of the leachate and slag phase is simple, reducing the difficulty of recovery. The water leaching method also avoids using acid and alkali in conventional leaching, reducing the cost and contributing to protecting the environment. The most significant advantage of the process is that the valuable metals to be recovered are recovered separately, avoiding the complex content of single component elements and reducing the difficulty of recovery. Meanwhile, the disadvantage of low purity of the product obtained by recovery is improved.

Then, 1.5 sodium carbonate was added to the spent catalyst and calcined at 900°C for 4 h. After the reaction, NiAl<sub>2</sub>O<sub>4</sub> and α-Al<sub>2</sub>O<sub>3</sub> in the spent catalyst can be converted to NiO and soluble NaAlO<sub>2</sub>. Similarly, V was converted to Na<sub>3</sub>VO<sub>4</sub>, creating conditions for subsequent leaching. At the leaching temperature of 75°C, L/S of 7, and leaching time of 2 h, Al and V leaching ratios were 99.64% and 99.24%, respectively. Therefore, the efficient leaching of Al and V was achieved, and NiO was detached from NiAl<sub>2</sub>O<sub>4</sub>. The leaching solution and residue are recovered separately. First, the stoichiometric Ba(OH)<sub>2</sub> with V was added to the leaching solution to obtain Ba<sub>3</sub>(VO<sub>4</sub>)<sub>2</sub>. The γ-Al<sub>2</sub>O<sub>3</sub>

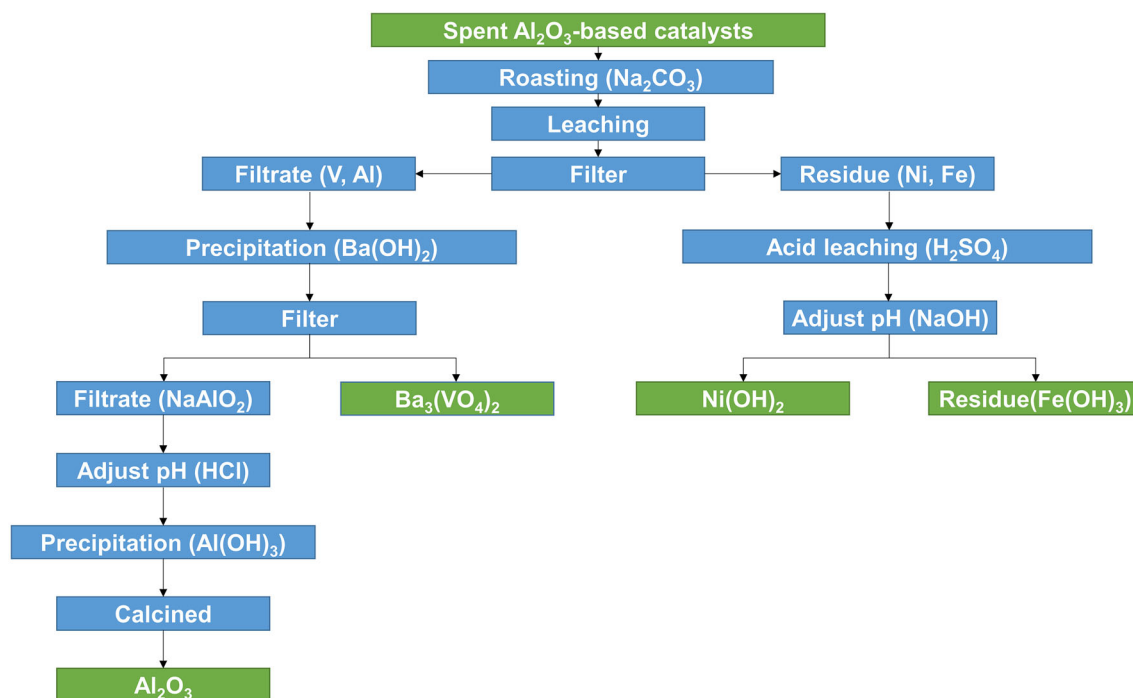


Fig. 10. Process flow diagram for the recovery of Al, Ni and V from spent Al<sub>2</sub>O<sub>3</sub>-based catalysts.

was obtained under roasting conditions at 800°C and can be used to re-prepare the catalyst. Then, continue to drop hydrochloric acid, and obtain precipitation and recovery. Second, sulfuric acid is used to leach Ni and Fe from the residue. Under the optimal conditions of 2 mol/L sulfuric acid and 60°C leaching temperature, the leaching rates of V and Fe are 98.22% and 98.44%. Subsequently, the solution was recovered by adding NaOH dropwise to fix the pH at 5. The product was calcined in a muffle furnace to obtain NiO.

### SUPPLEMENTARY INFORMATION

The online version contains supplementary material available at <https://doi.org/10.1007/s11837-023-05912-5>

### ACKNOWLEDGEMENTS

The present work was supported by the Liaoning Province Applied Basic Research Program Project 2023JH2/101300245, the National Natural Science Foundation of China (Grant No. 51974188), the Liaoning Revitalization Talents Program (Grant Nos. XLYC2008014), the Young Teachers Research Ability Cultivation Fund of Shenyang University of Technology (Grant No. QNPY202104), the Key Research Project Fund of Shenyang University of Technology (Grant No. X202167084), and Shenyang major scientific and technological achievements transformation special project (Grant Number 20-203-5-19).

### AUTHOR CONTRIBUTIONS

LL and YW developed the research direction and experimental plan. XL performed the experiments, obtained the experimental data, and wrote the first draft. JT revised the first draft. All participants were involved in the analysis of the experimental results and the revision of the manuscript.

### CONFLICT OF INTEREST

The authors declare that they have no known competing financial interests or personal relationships that could have appeared to influence the work reported in this paper.

### REFERENCES

1. Y. Ding, S. Zhang, B. Liu, H. Zheng, C.C. Chang, and C. Ekberg, *Resour. Conserv. Recycl.* 141, 284 <https://doi.org/10.1016/j.resconrec.2018.10.041> (2019).
2. S. Huang, J. Liu, C. Zhang, B. Hu, X. Wang, M. Wang, and X. Wang, *JOM* 71, 4681 <https://doi.org/10.1007/s11837-019-03741-z> (2019).
3. M. Razavian, S. Fatemi, and A.T. Najafabadi, *J. Environ. Chem. Eng.* 8, 103660 <https://doi.org/10.1016/j.jece.2020.103660> (2020).
4. W. Wang, L. Zhang, Y. Han, Y. Zhang, X. Liu, and S. Xu, *J. Clean. Prod.* 232, 266 <https://doi.org/10.1016/j.jclepro.2019.05.375> (2019).
5. M. Marafi, and A. Stanislaus, *Resour. Conserv. Recycl.* 52, 859 <https://doi.org/10.1016/j.resconrec.2008.02.004> (2008).
6. J. Willner, A. Fornalczyk, J. Cebulski, and K. Janiszewski, *Arch. Metall. Mater.* 59, 801 <https://doi.org/10.2478/amm-2014-0136> (2014).
7. M.K. Jha, J. Lee, M. Kim, J. Jeong, B.S. Kim, and V. Kumar, *Hydrometallurgy* 133, 23 <https://doi.org/10.1016/j.hydromet.2012.11.012> (2013).



8. S. Ilhan and D. Akgün, *J. Sustain. Metall.* 7, 470 <https://doi.org/10.1007/s40831-021-00351-5> (2021).
9. M. Marafi and A. Stanislaus, *Resour. Conserv. Recycl.* 53, 1 <https://doi.org/10.1016/j.resconrec.2008.08.005> (2008).
10. M.K. Nazemi and F. Rashchi, *Waste Manag. Res.* 30, 492 <https://doi.org/10.1177/0734242X11417984> (2012).
11. R. Banda, T.H. Nguyen, S.H. Sohn, and M.S. Lee, *Hydrometallurgy* 133, 161 <https://doi.org/10.1016/j.hydromet.2013.01.006> (2013).
12. S. Zhao, Z. Liao, Y. Xie, X. Li, Y. Dai, Z. Li, and M. Wang, *J. Sustain. Metall.* 7, 773 <https://doi.org/10.1007/s40831-021-00420-9> (2021).
13. B. Ghadai, P.C. Rout, D. Mohapatra, B. Padh, and B.Y. Reddy, *Hydrometallurgy* 191, 105237 <https://doi.org/10.1016/j.hydromet.2019.105237> (2020).
14. V. Ruiz, E. Meux, M. Schneider, and V. Georgeaud, *Ind. Eng. Chem. Res.* 50, 5307 <https://doi.org/10.1021/ie102428r> (2011).
15. Z. Zhao, M. Guo, and M. Zhang, *J. Hazard. Mater.* 286, 402 <https://doi.org/10.1016/j.jhazmat.2014.12.063> (2015).
16. D.J. Kim, H. Srichandan, C.S. Gahan, and S.W. Lee, *Can. Metall. Quart.* 51, 403 <https://doi.org/10.1179/1879139512Y.0000000031> (2012).
17. R.M. Gholami, S.M. Borghei, and S.M. Mousavi, *Hydrometallurgy* 106, 26 <https://doi.org/10.1016/j.hydromet.2010.11.011> (2011).
18. Y. Cai, L. Ma, X. Xi, Z. Nie, and Z. Yang, *Hydrometallurgy* 208, 105800 <https://doi.org/10.1016/j.hydromet.2021.105800> (2022).
19. B. Dash, I.N. Bhattacharya, B.V. Ramanamurthy, and R.K. Paramguru, *Korean J. Chem. Eng.* 28, 1546 <https://doi.org/10.1016/j.jhazmat.2021.125849> (2011).
20. M.N. Le and M.S. Lee, *Miner Process. Extr. Metall. Rev.* 42, 335 <https://doi.org/10.1080/08827508.2020.1726914> (2021).
21. S.P. Barik, K.H. Park, P.K. Parhi, and J.T. Park, *Hydrometallurgy* 111, 46 <https://doi.org/10.1016/j.hydromet.2011.10.001> (2012).
22. T.H. Nguyen and M.S. Lee, *J. Clean. Prod.* 90, 388 <https://doi.org/10.1016/j.jclepro.2014.11.048> (2015).
23. Y.C. Lai, W.J. Lee, K.L. Huang, and C.M. Wu, *J. Hazard. Mater.* 154, 588 <https://doi.org/10.1016/j.jhazmat.2007.10.061> (2008).
24. J.Z. Wang, S.N. Wang, A. Olayiwola, N. Yang, B. Liu, J. Weigand, M. Wenzel, and H. Du, *J. Hazard. Mater.* 416, 125849 <https://doi.org/10.1016/j.jhazmat.2021.125849> (2021).
25. H.R. Kim, J.Y. Lee, and J.S. Kim, *Korean Inst. Resour. Recycl.* 21, 65 <https://doi.org/10.7844/kiirr.2012.21.6.65> (2012).
26. X. Ye, S. Guo, W. Qu, S. Xu, L. Zhang, B. Liu, L. Wang, and C. Wang, *J. Taiwan Inst. Chem. E.* 97, 146 <https://doi.org/10.1016/j.jtice.2019.01.009> (2019).
27. H. Li, Y. Feng, H. Wang, H. Li, and H. Wu, *Sep. Purif. Technol.* 248, 117135 <https://doi.org/10.1016/j.seppur.2020.117135> (2020).
28. N. Kayal and N. Singh, *Chem. Central J.* 1, 1 <https://doi.org/10.1186/1752-153X-1-24> (2007).
29. J.A. Addlestone, *J. Phys. Chem.* 42, 437 <https://doi.org/10.1021/j100898a014> (2002).
30. L. Zhou, L. Li, N. Wei, and J. Li, *ChemCatChem* 7, 2508 <https://doi.org/10.1002/cctc.201500379> (2015).
31. I.S.S. Pinto and H.M.V.M. Soares, *Hydrometallurgy* 129, 19 <https://doi.org/10.1016/j.hydromet.2012.08.008> (2012).
32. J.W. Kim and H.G. Lee, *Metall. Mater. Trans. B.* 32, 17 <https://doi.org/10.1007/s11663-001-0003-0> (2001).
33. I.H. Choi, H.R. Kim, G. Moon, R.K. Jyothi, and J.Y. Lee, *Hydrometallurgy* 175, 292 <https://doi.org/10.1016/j.hydromet.2017.12.010> (2018).
34. M. Li, B. Liu, S.L. Zheng, S.N. Wang, H. Du, D.B. Dreisinger, and Y. Zhang, *J. Clean. Prod.* 149, 206 <https://doi.org/10.1016/j.jclepro.2017.02.093> (2017).
35. Y. Chen, Q. Feng, G. Zhang, L. Ou, and Y. Lu, *Min. Metall. Explor.* 24, 30 <https://doi.org/10.1007/BF03403355> (2007).
36. W. Huang, G. Liu, X. Li, T. Qi, Q. Zhou, and Z. Peng, *Mater. Lett.* 277, 128361 <https://doi.org/10.1016/j.matlet.2020.128361> (2020).
37. L.L. Zhang, Y.S. Wu, L.N. Zhang, Y.Z. Wang, and M.C. Li, *Vacuum* 133, 1 <https://doi.org/10.1016/j.vacuum.2016.08.005> (2016).
38. M. Marafi and A. Stanislaus, *Catal. Today* 178, 117 <https://doi.org/10.1016/j.catto.2011.07.001> (2011).
39. P.F. Xian, S.F. Zhou, M.Y. Wang, X.W. Wang, and B.F. Chen, *Trans. Nonferrous Metals Soc.* 27, 220 [https://doi.org/10.1016/S1003-6326\(17\)60025-6](https://doi.org/10.1016/S1003-6326(17)60025-6) (2017).
40. P. Lu, F. Liu, D.F. Xue, H. Yang, and Y.N. Liu, *Electrochim. Acta* 78, 1 <https://doi.org/10.1016/j.electacta.2012.03.183> (2012).
41. D. Peddis, S. Laureti, M.V. Mansilla, E. Agostinelli, G. Varvaro, C. Cannas, and D. Fiorani, *Superlattices Microstruct.* 46, 125 <https://doi.org/10.1016/j.spmi.2008.10.042> (2009).

**Publisher's Note** Springer Nature remains neutral with regard to jurisdictional claims in published maps and institutional affiliations.

Springer Nature or its licensor (e.g. a society or other partner) holds exclusive rights to this article under a publishing agreement with the author(s) or other rightsholder(s); author self-archiving of the accepted manuscript version of this article is solely governed by the terms of such publishing agreement and applicable law.